

Temporal Deconvolution study of Long and Short Gamma-Ray Burst Light curves

P.N. Bhat¹, Michael S. Briggs¹, Valerie Connaughton¹, Chryssa Kouveliotou², Alexander J. van der Horst⁴, William Paciesas¹, Charles A. Meegan⁴, Elisabetta Bissaldi³, Michael Burgess¹, Vandiver Chaplin¹, Roland Diehl⁶, Gerald Fishman², Gerard Fitzpatrick⁹, Suzanne Foley⁶, Melissa Gibby⁷, Misty M. Giles⁷, Adam Goldstein¹, Jochen Greiner⁶, David Gruber⁶, Sylvain Guiriec¹, Andreas von Kienlin⁶, Marc Kippen⁸, Sheila McBreen⁹, Robert Preece¹, Arne Rau⁶, Dave Tierney⁹ and Colleen Wilson-Hodge²

Received _____; accepted _____

¹University of Alabama in Huntsville, NSSTC, 320 Sparkman Drive, Huntsville, AL 35805, USA

²Space Science Office, VP62, NASA/Marshall Space Flight Center, Huntsville, AL 35812, USA

³Institute of Astro and Particle Physics, University Innsbruck, Technikerstr. 25, 6020 Innsbruck, Austria

⁴Universities Space Research Association, NSSTC, 320 Sparkman Drive, Huntsville, AL 35805, USA

⁶Max-Planck-Institut für extraterrestrische Physik (Giessenbachstrasse 1, 85748 Garching, Germany)

⁷Jacobs Technology, Inc., Huntsville AL 35806, USA

⁸Los Alamos National Laboratory, PO Box 1663, Los Alamos, NM 87545, USA

⁹School of Physics, University College Dublin, Belfield, Stillorgan Road, Dublin 4, Ireland

ABSTRACT

10

11

The light curves of Gamma-Ray Bursts (GRBs) are believed to result from internal shocks reflecting the activity of the GRB central engine. Their temporal deconvolution can reveal potential differences in the properties of the central engines in the two populations of GRBs which are believed to originate from the deaths of massive stars (long) and from mergers of compact objects (short). We present here the results of the temporal analysis of 42 GRBs detected with the Gamma-ray Burst Monitor onboard the Fermi Gamma-ray Space Telescope. We deconvolved the profiles into pulses, which we fit with lognormal functions. The distributions of the pulse shape parameters and intervals between neighboring pulses are distinct for both burst types and also fit with lognormal functions. We have studied the evolution of these parameters in different energy bands and found that they differ between long and short bursts. We discuss the implications of the differences in the temporal properties of long and short bursts within the framework of the internal shock model for GRB prompt emission.

12

Subject headings: Gamma-ray Bursts: general, GRBs: Long and Short GRBs, GRB

13

Light Curve Decomposition, GRB Central Engines

1. Introduction

14
 15 The temporal structure of GRB light curves exhibits very diverse morphologies, from
 16 single pulses to extremely complex multi-pulse structures. As a result, morphological
 17 GRB classification attempts have not been successful and the only established division
 18 of bursts into classes with different temporal characteristics is based on their durations
 19 (Kouveliotou, *et al.*, 1993). The latter have been found to distribute bimodally, with over
 20 75% of the events belonging in the long class (> 2 s) when durations are measured in the
 21 50-300 keV range. Since 1993 the GRB durations are mostly measured by their T_{90} (T_{50})
 22 intervals, the times during which 90% (50%) of the total event counts (or fluence) are
 23 collected (Kouveliotou, *et al.*, 1993). McBreen *et al.*, (1994) and later Horváth, (2002),
 24 showed that durations (T_{90}) of both long and short GRBs follow lognormal distributions
 25 separately. Several authors have studied the deconvolution of GRB light curves into their
 26 constituents, and have shown that in general, these are discrete, often overlapping pulses
 27 with durations ranging from a few milliseconds to several seconds and almost always
 28 asymmetric shapes, with faster rises than decays (Norris *et al.*, 1996; Hakkila and Preece,
 29 2011). These highly varied GRB temporal profiles are suggestive of a stochastic process
 30 origin.

31 Two distinct mechanisms have been proposed to explain the origin of pulses in GRBs.
 32 In the external shock model, radiation pulses are emitted when a relativistic shell ejected
 33 by the GRB central engine is decelerated by the circum-burst material (Mészáros and Rees,
 34 1993). A homogeneous medium leads to a single pulse but an irregular, clumpy
 35 environment can produce a complex profile if a large number of small clouds are present
 36 (Dermer and Mitman, 1999). According to the internal shock model (Rees and Mészáros,
 37 1994), the central engine generates relativistic shells with highly non-uniform distribution
 38 of Lorentz factors and the pulses are formed by the collision between a rapidly moving

39 shell with a slower shell. Thus in principle the variability of the GRB light curves may
40 directly correspond to the activity of their central engines (Daigne and Mochkovitch, 2003;
41 Nakar and Piran, 2002). Hence the studies of pulse properties are important to determine
42 whether GRB sources require engines that are long lasting or impulsive (Dermer, 2004).

43 Investigations linking GRB properties with their pulse characteristics have already been
44 carried out by several authors (Norris *et al.*, 1996; Li and Fenimore, 1996; Quilligan *et al.*,
45 1999; Lee, Bloom and Petrosian, 2000; McBreen *et al.*, 2001; Hakkila and Cumbee, 2008).
46 Norris *et al.*, (1996) were the first to deconvolve the profiles of long and bright GRBs
47 detected with the Burst And Transient Source Experiment (BATSE) onboard the Compton
48 Gamma Ray Observatory (*CGRO*) into pulses and study the pulse shape parameters as a
49 function of energy. Gupta *et al.*, (2000) were the first to fit lognormal functions to pulses
50 in short GRBs detected with BATSE. McBreen *et al.*, (2001) applied a pulse identification
51 algorithm on a set of BATSE short bright bursts and derived their pulse shape parameters;
52 they concluded that the pulse rise and decay times follow lognormal distributions. However,
53 the BATSE GRB light curves used in these studies had a time resolution of 64 ms for long
54 bursts, which could have masked narrower pulses in those bursts. However the short burst
55 studies have been carried out using higher resolution data.

56 A long standing question has been, therefore, whether the representative time scales
57 associated with pulses of long GRBs form a separate class from those in short bursts
58 perhaps reflecting the two different prevalent models for their origin, i.e., long bursts
59 originate from the collapse of massive stars (Woosley and Heger, 2006; Woosley and Bloom,
60 2006), while short GRBs result from the merger of two compact objects (Eichler *et al.*, 1989;
61 Narayan *et al.*, 1992). If we could deconvolve the GRB light curves in terms of simpler pulse
62 shapes, we could potentially identify the differences in the central engines of long and short
63 GRBs. In this paper, we show that there is a fairly high degree of determinism underlying

64 the complex nature of the GRB temporal profiles. In § 2 we describe the instrument and
65 the selection criteria for our sample, and in § 3 we expand on our analysis technique. In § 4
66 we decompose the high-time resolution GRB data of the Gamma-ray Burst Monitor (GBM)
67 onboard the *Fermi* Gamma-ray Space Telescope (hereafter *Fermi*) into individual pulses
68 and examine the distributions of the pulse shape parameters for long and short duration
69 GRBs. Further we apply the same analysis technique to GRB light curves in various energy
70 bands and study the pulse shape evolution with energy. We discuss our results in § 5.

71 **2. Instrumentation and Data Selection**

72 GBM is an uncollimated all-sky (field of view ≥ 8 sr) monitoring instrument. It
73 consists of an array of 12 NaI(Tl) scintillation detectors mounted in clusters of three around
74 the spacecraft. Each NaI(Tl) detector is 12.7 cm in diameter by 1.27 cm thick, and covers
75 an energy range from 8 keV to 1 MeV. In addition, GBM includes two Bismuth Germanate
76 (BGO) detectors, each 12.7 cm in diameter by 12.7 cm thick, placed on either side of *Fermi*.
77 The BGOs cover energies above 150 keV up to a maximum of 40 MeV (Meegan *et al.*,
78 2009).

79 The GBM on-board software incorporates burst triggering on time scales as short as
80 16 ms. All triggers generate time-tagged event data (TTE) consisting of the photon arrival
81 time and energy as deposited from each of the 14 detectors with a temporal resolution of
82 $2 \mu\text{s}$ (Meegan *et al.*, 2009). The very high temporal resolution and large energy band-width
83 are major assets for the study of GRBs in general and the study of short events, in
84 particular. A pre-burst ring buffer saves about half a million events before the trigger,
85 which corresponds to a time interval of ~ 30 seconds. The TTE data are produced for
86 ~ 300 seconds after the trigger. All short bursts and a bulk of the long bursts have full
87 temporal coverage by TTE data. The energy range for both NaI and BGO detectors is

88 digitized into 128 channels, pseudo-logarithmically spaced to provide channel widths less
 89 than each detector energy resolution up to 12 MeV though TTE data are available at
 90 coarser resolution up to 40 MeV. During the 3 years since its launch (2008 June 11) GBM
 91 has collected over 700 GRBs. During the first year GBM detected 225 GRBs of which 59
 92 were BGO bright bursts (Bissaldi, *et al.*, 2011). This is to ensure the burst is sufficiently
 93 hard to allow pulse decomposition analysis in different energy channels. Out of the latter
 94 dataset we chose long bursts with the product of fluence and peak flux (1.024s) values
 95 greater than 1.0×10^{-4} and 5.0×10^{-6} erg ph/cm⁴/s for long and short bursts respectively.
 96 Burst fluences and peak fluxes estimated in the energy range 10-1000 keV are taken from
 97 the GBM Gamma-ray burst catalog (Paciesas, *et al.*, 2011). As a result, the final sample
 98 includes 32 long bursts with fluences ranging from 5.5×10^{-6} to 2.7×10^{-4} erg/cm² and
 99 10 short bursts with fluences ranging from 8.5×10^{-7} to 8×10^{-6} erg/cm². This unusual
 100 selection criteria is simply to eliminate weak and long bursts with fluences above the
 101 threshold that are difficult for the pulse decomposition analysis. We have also used the
 102 BGO data in the current analysis. The burst durations and the number of fitted pulses
 103 are listed in Table 1. Possible selection effects arising from our choice of burst sample is
 104 assumed to be small in the present analysis.

105 For each burst we summed the TTE data of the four NaI detectors that registered the
 106 highest gamma-ray signal (with an angle to the burst direction of $\leq 60^\circ$) to derive their
 107 light curves with a resolution of 1 ms. In the case of BGO detectors, the light curves from
 108 both the detectors were summed. Each light curve included the entire burst and background
 109 regions up to about 10-20 s before and after the burst. We varied the temporal resolution
 110 used for the analysis depending on the burst intensity (see next section for details). The
 111 analysis described below was performed on the entire energy range of NaI (8 – 1000 keV)
 112 and BGO (0.15 – 45.0 MeV) detectors as well as in six NaI energy ranges per burst (8 – 520
 113 keV; see also Table 2). It may be noted that there are uncertainties in the energy edges

114 listed in Table 2 that arise primarily from the finite energy resolution of the GBM detectors
115 (Meegan *et al.*, 2009).

116

3. Analysis Technique

117 In general, a parameter which can be written as a product of ≥ 3 random variables
118 tends to follow a lognormal function (Aitchison and Brown, 1969). Since the pulse
119 shape parameters of GRB light curves can be described as such a product, we were
120 motivated to use a similar procedure to test this hypothesis (Ioka and Nakamura, 2002).
121 Ioka and Nakamura, (2002) argue that the distribution of a product of variables tends to
122 the lognormal distribution as the number of multiplied variables increases, the distribution
123 of pulse width may be closer to the lognormal distribution than that of the pulse intervals
124 between successive pulses. It has already been shown that the long and short GRB
125 durations, the time interval between successive pulses (McBreen *et al.*, 1994), fluence and
126 pulse intervals between successive pulses within each burst (Li and Fenimore, 1996), pulse
127 durations (Nakar and Piran, 2002) and spectral break energies (Preece, *et al.*, 2000) do
128 follow lognormal distributions.

129 We also choose a lognormal function to fit pulses in a GRB light curve. A lognormal
130 function in this case has 4 free parameters, namely the amplitude (A), mean (μ), standard
131 deviation (σ) and time. The advantage of choosing this functional form is that it converges
132 in all cases even when the shape of the light curve is very complex, where the pulses are
133 often overlapping. The pulse shape parameters are derived from the fit parameters using
134 the following formulations.

135 A lognormal function is represented as:

$$f(x) = \begin{cases} \frac{A}{\sqrt{2\pi x\sigma}} \exp\left[-\frac{(\log \frac{x-\mu}{2\sigma^2})^2}{2\sigma^2}\right] & \text{if } x > 0 \\ 0 & \text{if } x \leq 0 \end{cases}$$

136 where, μ and σ are the sample mean and standard deviation of $\log x$, and A is the
 137 amplitude. The rise time, τ_r , decay time, τ_d , and the full width at half maximum of each
 138 pulse, FWHM, can be derived from the fit parameters of the lognormal function given
 139 above. The rise and decay times are measured from the time differences at 10% and 90% of
 140 the peak amplitude of a pulse.

$$\tau_r = \exp(\mu - \sigma^2) \left[\exp\left(-\sigma\sqrt{2\log\left(\frac{10}{9}\right)}\right) - \exp\left(-\sigma\sqrt{2\log(10)}\right) \right]$$

$$\tau_d = \exp(\mu - \sigma^2) \left[\exp\left(\sigma\sqrt{2\log(10)}\right) - \exp\left(\sigma\sqrt{2\log\left(\frac{10}{9}\right)}\right) \right]$$

$$FWHM = \exp(\mu - \sigma^2) \left[\exp\left(\sigma\sqrt{2\log(2)}\right) - \exp\left(-\sigma\sqrt{2\log(2)}\right) \right]$$

141 For each GRB we initially selected the number of possible pulses contained in the light
 142 curve by visually identifying the significant valleys on either side of a pulse. This process
 143 was repeated for each burst varying the temporal resolution of the summed light curve until
 144 the number of valleys reached a maximum. If the resolution was too fine, the pulses were
 145 buried in statistical fluctuations and hence the number of identified valleys was too small.
 146 At very coarse resolutions the closely spaced pulses merged with each other also resulting in
 147 a reduced number of valleys. The number of valleys is maximum at the optimum temporal
 148 resolution for a given burst. Figure 1 shows such a histogram where the number of valleys
 149 identified automatically by a routine based on the technique of Li and Fenimore, (1996),

150 as a function of bin-width of GRB light curve. The number of valleys increases initially
151 with increasing binwidth and then reaches a broad maximum at a resolution in the range
152 25-50 ms and then falls gradually with further increase in the bin-width. The number
153 valleys estimated manually for this burst was 18 at a chosen optimum bin-width of 50 ms
154 which agrees well with those estimated objectively. The mean time resolution for all the
155 GRBs in our sample is ~ 40 msec.

156 The array of valleys was then used as input to the pulse fitting routine. It generates
157 initial guesses of the amplitudes, means and the standard deviations based on the number
158 of counts in the light curve between a pair of valleys while the pair of valleys are used
159 to estimate the initial guess of time parameter. The routine then simultaneously fits
160 lognormal functions to pulses at optimum times and a quadratic to the background. It
161 compared the model light curve with the data and minimized its χ^2 value by varying the
162 pulse shape parameters and the position of the pulses. The goodness of fit, n , was finally
163 calculated by computing the likelihood parameter as $-2\ln \mathcal{L}$ (which approaches Pearson's χ^2
164 for large model values) divided by the number of degrees of freedom (dof). The number
165 of dof is the difference between the number of data points in the light curve minus the
166 total number of fitted parameters. This procedure was then repeated for the light curves
167 in the first four to six energy bands (depending on the burst intensity in the higher energy
168 bands) shown in Table 2, defined so that a typical GRB light curve had similar signal to
169 noise ratio in each channel. After pulse fitting we used the pulse mean positions to compute
170 the intervals between successive pulses, while the variation of the pulse shape parameters
171 in different energy bands were used to study the spectral evolution of the pulse shapes.
172 The pulse mean positions refer to the mean times (with respect to the trigger time) of the
173 lognormal pulses.

174 To test the integrity of the fit we computed a weight for each of the fitted pulses in a

175 light curve by estimating the percentage change in the goodness of fit parameter with that
 176 pulse excluded. Pulses with weights less than 2% were excluded from the fit as they most
 177 likely were due to statistical fluctuations. The overall goodness of fit did not change more
 178 than 10% compared to its value before any pulse rejection. No case was found where an
 179 additional pulse was needed to improve the residuals. Thus the pulse fitting procedure was
 180 optimized to ensure removal of spurious pulses.

181 To check the robustness of our fits, we also performed a series of simulations as follows.
 182 We chose a set of pulses fitted to a light curve and generated a synthetic light curve using
 183 these pulses superposed over the burst fitted background. We then reduced the light curve
 184 intensity in steps of 10%, starting at 100%, and added statistical noise to each bin. Each
 185 light curve was fitted by the normal procedure and recovered entirely until the intensity
 186 was decreased to 50%. The degree of percentage recovery declined thereafter, and reached
 187 75% of the original, when the intensity was reduced to 10% of the total. We concluded that
 188 the fit is robust for a large range of burst intensities.

189 Further we reduced the duration of the simulated burst by a factor and fitted the
 190 light curve with the lognormal functions as before. Each time the separation between the
 191 pulses too reduced by the same factor. Hence there was no lower limit on the inter-pulse
 192 separation caused by the closeness of the successive peaks in the light curve. This was
 193 tested by reducing the burst duration by a factor of 1000.

194 Finally, to address the issue of the interdependency of the rise and decay times of a
 195 lognormal function we tried two new functions, where these times can vary independently.
 196 They are:

$$197 \quad f_1(x) = \frac{A}{(\tau_d - \tau_r)} \left[\exp\left(-\frac{x}{\tau_r}\right) - \exp\left(-\frac{x}{\tau_d}\right) \right], \text{ (Leo, 1994)}$$

$$198 \quad f_2(x) = A\lambda \exp\left(-\frac{\tau_1}{x} - \frac{x}{\tau_2}\right) \text{ for } x > 0, \text{ (Norris } et \text{ al., 2005)}$$

199 where $\lambda = \exp(2\mu)$ and $\mu = \left(\frac{\tau_1}{\tau_2}\right)^{\frac{1}{2}}$.

200 We find that for long bursts with a small number of pulses, both the above functions
 201 fit the light curve as well as the lognormal function. However, in case of bursts with
 202 complex light curves consisting of several overlapping narrow pulses, these functions fit
 203 poorly resulting in large χ^2 compared to a fit with a lognormal function. Since the present
 204 analysis aims at a comparison of the pulse properties of long and short bursts, we opted to
 205 use the lognormal function, which describes the light curve best in all cases.

206 4. Results

207 We performed the analysis described above on all 42 GRBs in our sample. The pulse
 208 shape parameters from the analyses of the entire sample of light curves used here are
 209 summarized in 2 tables which are available in the online version of this paper. Figure 2
 210 shows an example of fitted pulses to light curves of one long (GRB080723D, upper plot)
 211 and one short (GRB090227B, lower plot) GRB. The quality of each fit, n , is indicated at
 212 the top right hand corner of each panel. The mean value of this parameter for all the 42
 213 fits is 1.15 with a standard deviation of 0.13. Figure 3 shows the distribution of n . We note
 214 that it peaks around 1, as expected since n is expected to follow the χ^2 distribution.

215 4.1. Pulse shape parameters

216 For each burst, we derived τ_r , τ_d and $FWHM$ for every fitted pulse from the formulae
 217 listed in the previous section. Figure 4 shows the distributions of pulse FWHM for long and
 218 short bursts also independently fitted with lognormal functions with mean values of pulse
 219 widths of 0.95 s and 0.06 s, respectively. The distributions are overlapping but distinct for

220 the two types of bursts. We note that short burst light curves consist of distinctly narrower
 221 pulses compared to long GRBs.

222 The pulse widths and intervals between successive pulses are primary attributes
 223 which could ultimately reveal important clues about GRB physics. Figure 5 shows the
 224 distributions of the time intervals (Δt) between adjacent pulse positions for long and short
 225 GRBs. Again we fit the distributions independently with lognormal functions. The means
 226 of the fitted lognormal functions are 1.6 s and 0.08 s for long and short bursts, respectively.
 227 The pulses in short bursts are about 20 times more closely spaced than those in the long
 228 bursts. The range of intervals between successive pulses spans nearly 3 decades both for
 229 long and short GRBs consistent with the earlier results for BATSE bursts (Norris *et al.*,
 230 1996). An exponential function does not fit the cumulative distributions of the intervals
 231 between successive pulses well, indicating that most likely the GRB pulses do not follow a
 232 Poisson distribution in time.

233 It may be noted that the average redshift of short bursts is smaller than that of long
 234 bursts (see section 5). Hence the average pulse widths and intervals between successive
 235 pulses of long bursts could be larger by a factor of 1.74 because of this effect. However the
 236 redshift effect is too small to account for the separation between them as seen in figures 4
 237 and 5.

238 To compare the pulse width contribution to the total duration in short and long
 239 bursts, we derive the ratio of the pulse width (FWHM) to the T_{90} of each burst. Figure
 240 6 (top panel) shows the histograms of these ratios for long and short bursts. Also shown
 241 are the median values of these distributions. The same figure (lower panel) shows similar
 242 distributions for the ratio of the pulse time intervals between successive pulses and the
 243 burst durations again for both burst types. The distributions for long and short bursts are
 244 overlapping and consistent with each other, considering large uncertainties in the short

245 burst durations (Table 1). In order to quantify the degree of overlap we estimated the time
 246 lag between the two distributions as follows. We estimate the cross-correlation coefficient
 247 (CC) as a function of lag between the two histograms. It is found that maximum of the CC
 248 values are 0.94 and 0.91 respectively for the distributions implying that the corresponding
 249 distributions for long and short bursts are correlated. The lag is defined as its value where
 250 the CCF peaks. In addition, we estimated lag 100 times for each pair of histograms while
 251 adding Poisson noise to the data each time. The standard deviation of the lags from
 252 the simulated histograms is the error on the estimated lag. The lags so estimated are
 253 1.0 ± 0.7 bins and 2.0 ± 0.7 bins for the two distributions respectively. The values of lags are
 254 close to zero supporting the general observation that the short GRBs are similar to long
 255 GRBs compressed in time (Guiriec, *et al.* 2010).

256 We now compare the GBM results with those of the BATSE bursts. Nakar and Piran,
 257 (2002) use a modified peak finding algorithm first reported by Li and Fenimore, (1996), to
 258 a sample of 68 long BATSE bursts and report that the pulse durations follow a lognormal
 259 distribution. The pulse interval distribution which peaks around an interval of 1.0 s
 260 also exhibits an excess of longer intervals between successive pulses with respect to a
 261 lognormal function. This is consistent with the analysis of 319 long bright BATSE GRBs
 262 by Quilligan *et al.*, (2002). They show that for long GRBs the distribution of intervals
 263 between successive pulses peak at 1 s and intervals longer than 15 s, which form 5% of the
 264 total, do not fit the lognormal distribution. They also show that these intervals between
 265 successive pulses are consistent with a power law. The origin of this excess has been
 266 attributed to the existence of quiescent times between successive peaks. In the present
 267 data, the distribution of pulse intervals for long bursts peaks around 1 s and the fraction
 268 of intervals between successive pulses above 15 s is $(3.8 \pm 0.8)\%$ which is consistent with
 269 the above result. The interval distributions for both long and short bursts are best fit by
 270 lognormal functions (Figure 5). The lognormal fit for long bursts shows a hint of an excess

271 of long intervals between successive pulses even though statistically not compelling because
 272 of smaller number of bursts in our sample.

273 Nakar and Piran, (2002) find a positive correlation ($> 70\%$) between pulse width and
 274 the preceding interval and a weaker correlation between pulse width and the following time
 275 interval. They considered only bursts with more than 12 well separated pulses and the total
 276 number of long bursts in their sample meeting this criteria was 12. There are 7 long bursts
 277 meeting these criteria in our sample. A search for such a correlation in our GRB sample has
 278 been carried out. In addition, we also searched for possible correlations between the pulse
 279 amplitude and the preceding or following time interval. We found one case of significant
 280 correlation (for GRB090626A) between the pulse width (FWHM) and the following time
 281 interval between successive pulses. The Pearson’s linear correlation coefficient is 0.896 with
 282 a statistical null hypothesis probability of 2.42×10^{-4} . The corresponding plot is shown in
 283 Figure 7. We found good correlations in a few other cases. However these correlations were
 284 found to be contributed by one or two deviant points and hence likely to be spurious. No
 285 significant correlations were found between the pulse amplitude and the time intervals in
 286 any burst in our limited sample. It seems that there are certain types of long bright GRBs
 287 which show such correlation between the pulse width and following time interval between
 288 successive separable pulses. The implications of these correlations is not clear at present.

289 4.2. Spectral Evolution of Pulse Shape Parameters

290 Figure 8 shows a set of light curves of GRB 090626A in 7 different energy bands. Here
 291 we were restricted by the statistics in the higher energy channels, which did not allow
 292 reliable pulse fitting beyond 524 keV for many bursts. The histograms of the pulse shape
 293 parameters were generated as above in each energy range for short and long bursts. We
 294 assigned a mean energy for each range estimated as the geometric mean of the energy

295 boundaries of each band. The energy range of each light curve is indicated on each plot.
 296 The bottom panel is from a fit to the BGO light curve of the same burst in the entire BGO
 297 energy range. As in figure 2 the individual pulses shown at the bottom of each panel when
 298 superposed on the quadratic background (shown as dashed line) describe the burst light
 299 curve shown as continuous line in red. Table 3 lists the number of pulses fitted for a sample
 300 of long GRBs in different energy bands. There does not seem to be a drastic change in the
 301 number of fitted pulses in the NaI energy range. The pulse fitting analysis of the BGO light
 302 curves in various energy bands were limited to very few bursts and hence the results from
 303 the analysis of full energy light curves only are used here.

304 Figure 9 shows the distributions of pulse width (FWHM) of long and short GRBs
 305 in different energy ranges. The distributions in each energy band are well fit (shown as
 306 continuous curves) by lognormal functions. The width of the fitted lognormals, as well as
 307 the values where the distributions peak, do not seem to change significantly with energy.
 308 The largest differences appear when we compare the two extreme energy bands, namely
 309 between 18 keV and ~ 3.15 MeV, with the latter widths being 0.04s and 0.5s narrower, for
 310 short and long GRBs, respectively.

311 Figure 10 shows the evolution of the distributions of time intervals between neighboring
 312 pulses of long and short bursts. Also shown are the best-fit lognormal functions in each
 313 energy band both for long and short GRBs. Figure 11 shows the variation of the median
 314 pulse width (FWHM) and median time interval between successive pulses as a function of
 315 increasing energy for long and short bursts. We note marked differences in the evolution
 316 of these 2 parameters for the two types of bursts. In both cases the short bursts show a
 317 relatively rapid decrease with energy as compared to long GRBs in agreement to earlier
 318 results where a general tendency of GRB pulses to be narrower at higher energies has been
 319 identified (Norris *et al.*, 1996). The energy dependence of median pulse widths can be

320 represented as $\Delta t \propto E^{\alpha_w}$ where $\alpha_w = 0.07 \pm 0.03$ for long bursts, while $\alpha_w = -0.2 \pm 0.1$
 321 for short bursts. The median pulse interval also evolves very differently in the case of long
 322 and short bursts. Both show a power law dependence, with the exponents for long and
 323 short GRBs being $\alpha_{\Delta t} = 0.003 \pm 0.02$ and $\alpha_{\Delta t} = -0.16 \pm 0.05$, respectively. The slope for
 324 long GRBs is consistent with zero, indicating that the median interval size is constant with
 325 energy, while the short GRB pulses are more closely spaced at higher energies.

326 5. Discussion

327 Sari & Piran (1997) argued that the observed temporal structure of a GRB reflects
 328 the activity of the central engine that generates it. According to the internal shock model,
 329 the GRB pulses are formed by the collisions among relativistic shells ejected by the central
 330 engine with a distribution of Lorentz factors (γ_e). A GRB pulse shape depends on three
 331 time scales. The hydrodynamic time scale, t_{dyn} (that determines the pulse rise time), the
 332 angular spreading time scale, t_{ang} (that determines the pulse decay time), and the cooling
 333 time scale, t_{rad} (which is usually much shorter than the other two and can be ignored)
 334 (Kobayashi, *et al.*, 1997; Katz, 1997; Fenimore *et al.*, 1996). Hence the measured pulse
 335 shape parameters have the potential to diagnose the pulse characteristics such as the bulk
 336 Lorentz factors, γ_e , shell radii and thicknesses (Kocevski *et al.*, 2003).

337 Because of relativistic radiation-beaming only a small cone of opening angle γ_e^{-1} is
 338 visible to the observer. The time difference between γ -rays emitted on-axis and off-axis
 339 constitutes the pulse decay. The off-axis γ -rays are delayed by $T_{ang} = \frac{R_e}{2\gamma_e^2}$, where R_e is
 340 the typical radius characterizing the emission shell (Nakar, 2007). The decay times of short
 341 GRBs are shorter than those of the long ones. Assuming an internal shock origin for both,
 342 we consider the possible implications of our observational results. If the curvatures of the
 343 emitting shells (R_e) are similar for both GRB types, then shorter decay times would imply

344 that the γ -ray emitting shells of short bursts have significantly larger Lorentz factors. On
 345 the other hand if the Lorentz factors are similar then the radii of the emitting shells are
 346 smaller in short GRBs, implying a more compact central engine. Ackermann et al. (2010)
 347 compare the estimates of Γ_{\min} (the bulk Lorentz factors) for two long and one short GRBs.
 348 These are 900, 1000 and 1218, respectively, possibly indicating (albeit with small number
 349 statistics) that the shell radii of short GRBs are significantly smaller.

350 According to Dermer and Menon, (2009) the GRB central engine releases energy at
 351 a fixed rate over a time scale Δ_0/c , where Δ_0 is a characteristic size scale of the engine.
 352 Assuming that the shortest time scale in GRB prompt emission is the shortest pulse
 353 width, we can estimate the length scale of the GRB central engine. Using the mean
 354 shortest FWHM of short and long GRBs, 0.016 s and 0.087 s, respectively, we find their
 355 corresponding length scales to be 4.8×10^8 cm and 2.6×10^9 cm, respectively in the observer
 356 frame. To convert these length scales to the source frame, we use the mean redshifts,
 357 $z = 2.245, 0.862$, of 151 long and 12 short *Swift* GRBs¹. These are 8×10^8 cm and 2.6×10^8
 358 cm, respectively. According to the GRB standard model (Mészáros, 2006) the above
 359 length scales agree with the saturation radius of the fireball ($\sim 10^9$ – 10^{10} cm), *i.e.*, the radius
 360 signifying the end of the acceleration phase and the beginning of the coasting phase of the
 361 Lorentz factor γ_e . Our results imply that the central engines of short GRBs seem to have a
 362 relatively smaller saturation radii.

363 We now estimate the rest frame radii of the shells, which give rise to the pulses.
 364 According to Dermer, (2004) the radius of the emission shell R_e is given by:

$$R_e \approx \frac{2\gamma_e^2 ct_{var}}{1+z}$$

365 where t_{var} is the GRB light curve variability time scale. We substitute t_{var} with the mean

¹http://swift.gsfc.nasa.gov/docs/swift/archive/grb_table/

366 FWHM values of the GRB pulses (which are 0.9 and 0.06 s for long and short bursts
 367 respectively) and assuming a typical value for $\Gamma_e \approx 1000$, we find that the mean shell radii
 368 are 1.7×10^{16} cm and 1.9×10^{15} cm for long and short bursts, respectively. Zhao, Li and Bai,
 369 (2011) find shell radii for the long GRB 080916C that are slightly larger but comparable to
 370 the above mean value. Even larger prompt emission radii were inferred for other GRBs by
 371 different estimates (Kumar *et al.*, 2007; Racusin, 2008). Our mean shell radii agree with
 372 the radial distances when the internal shock phase ($\sim 10^{14-15}$ cm) or the prompt emission
 373 starts (Mészáros, 2006), possibly indicating that the beginning of the internal shock phase
 374 occurs earlier for short bursts.

375 If the individual pulses in the GRB light curves are indeed formed by the collision
 376 of shells with unequal Lorentz factors (Rees and Mészáros, 1994; Nakar and Piran, 2002)
 377 then shorter intervals between pulses (Figure 5) imply that the relativistic shells are more
 378 frequent. However, the longer intervals between successive pulses and durations of long
 379 GRBs indicate that the central engine shell ejection persists for longer times. In other
 380 words, the duration as well as the structure of the light curve are indeed related to the
 381 central engine activity.

382 Temporal analysis of long and short GRB light curves carried out here supports the
 383 general observation that the short bursts are temporally similar to long ones but compressed
 384 in time, which could be related to the nature of the central engine of the respective bursts.

385 6. Acknowledgments

386 The GBM project is supported by the German Bundesministerium für Wirtschaft und
 387 Technologie (BMWi) via the Deutsches Zentrum für Luft- und Raumfahrt (DLR) under the
 388 contract numbers 50 QV 0301 and 50 OG 0502.

389 AJvdH was supported by NASA grant NNH07ZDA001-GLAST.

390 SMB acknowledges support of the Union Marie Curie European Reintegration Grant
391 within the 7th Program under contract number PERG04-GA-2008-239176.

392 SF acknowledges the support of the Irish Research Council for Science, Engineering
393 and Technology, cofunded by Marie Curie Actions under FP7.

394 We also acknowledge the constructive comments and suggestions from the anaonymous
395 referee which improved the quality of presentation.

Table 1. List of GRBs, chosen for the present analysis. Also listed are their durations (column 2) and the number of fitted pulses (column3)

Burst #	Duration T_{90} (s)	# of Fitted Pulses
Long GRBs		
bn080723557	58.37 ± 1.98	29
bn080723985	42.80 ± 0.66	18
bn080807993	19.07 ± 0.18	16
bn080817161	60.29 ± 0.47	14
bn080825593	20.99 ± 0.23	20
bn080906212	2.875 ± 0.77	5
bn080916009	62.98 ± 0.81	32
bn080925775	31.74 ± 3.17	15
bn081009690	176.2 ± 2.13	5
bn081101532	8.260 ± 0.90	7
bn081110601	17.34 ± 0.68	2
bn081121858	41.98 ± 8.51	9
bn081122520	23.30 ± 2.11	6
bn081125496	9.280 ± 0.61	4
bn081129161	62.66 ± 7.32	2
bn081207680	97.28 ± 2.35	3
bn081215784	5.570 ± 0.14	10
bn081224887	16.45 ± 1.16	4

Table 1—Continued

Burst #	Duration T_{90} (s)	# of Fitted Pulses
bn081231140	28.74 ± 2.61	3
bn090102122	26.62 ± 0.81	25
bn090131090	35.07 ± 1.06	8
bn090217206	33.28 ± 0.72	23
bn090323002	135.2 ± 1.45	17
bn090328401	61.70 ± 1.81	7
bn090424592	14.14 ± 0.26	15
bn090425377	75.39 ± 2.45	3
bn090528516	79.04 ± 1.09	16
bn090529564	9.850 ± 0.18	7
bn090618353	112.4 ± 1.09	20
bn090620400	13.57 ± 0.72	5
bn090623107	47.11 ± 2.57	18
bn090626189	48.90 ± 2.83	24
Short GRBs		
bn080905499	0.960 ± 0.35	7
bn081209981	0.192 ± 0.14	2
bn081216531	0.768 ± 0.43	7
bn090227772	1.280 ± 1.03	5

Table 1—Continued

Burst #	Duration T_{90} (s)	# of Fitted Pulses
bn090228204	0.448 ± 0.14	9
bn090305052	1.856 ± 0.58	10
bn090308734	1.664 ± 0.29	7
bn090429753	0.640 ± 0.47	3
bn090510016	0.960 ± 0.14	12
bn090617208	0.192 ± 0.14	3

Table 2: The lower edges of the 8 energy channels used for pulse fitting of GRB light curves using the 2 types of GBM detectors. The upper energy edge of channel 7 is assumed to be twice the lower energy edge of that channel.

Channel #	0	1	2	3	4	5	6	7
NaI (keV)	8.0	20	40	70	142	270	524	>985
BGO (MeV)	0.11	0.28	0.55	1.4	3.3	7.2	19.2	>45.5

Table 3: The variation of the number of fitted pulses in various NaI energy ranges for a sample of long bursts.

NaI Energy Range (keV)	8-20	20-40	40-70	70-142	142-270	270-524
Mean Energy (keV)	12.5	28.3	53.5	100.0	195.6	376.1
bn081207680	2	2	2	2	2	2
bn081215784	8	9	9	9	8	8
bn081231140	3	3	3	3	3	2
bn090217206	19	20	23	26	19	19
bn090323002	18	16	20	26	20	18
bn090328401	6	6	4	5	6	5
bn090424592	13	15	16	17	14	11
bn090529564	7	8	6	9	8	6
bn090618353	23	22	24	26	30	24
bn090626189	30	33	32	32	26	20

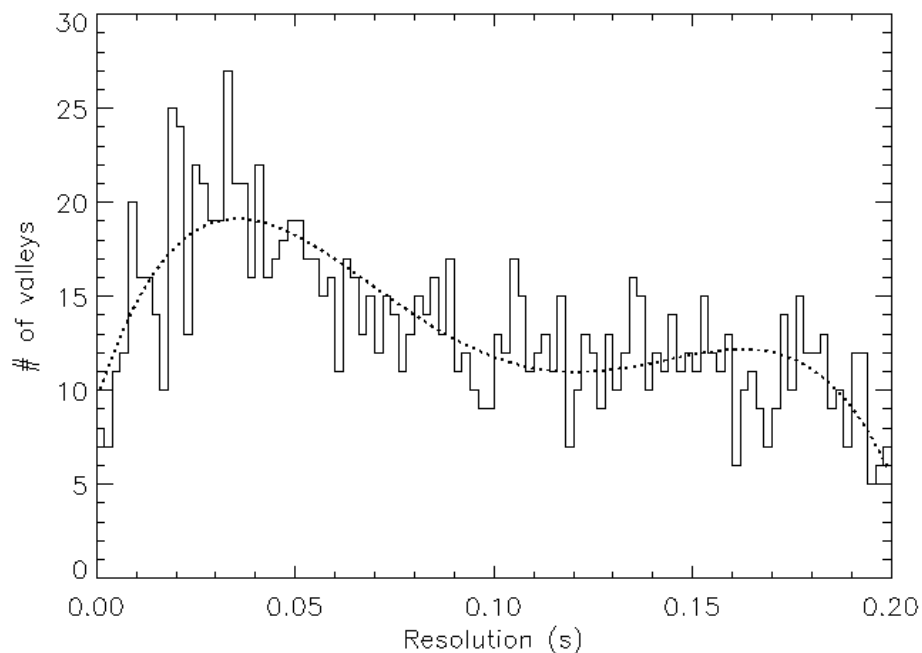


Fig. 1.— A sample histogram of the number of valleys identified by an algorithm based on the method suggested by Li and Fenimore, (1996), as a function of bin-width of the light curve for GRB 080723D. The number of valleys increases initially and reaches a broad maximum at the optimum bin-width (25-50 ms) and then gradually falls at very coarse resolution. The curve is a polynomial fit to guide the eye only. The number of valleys and the bin-width at the maximum agrees with that chosen for this GRB which is 18 valleys at a time resolution of 50 ms.

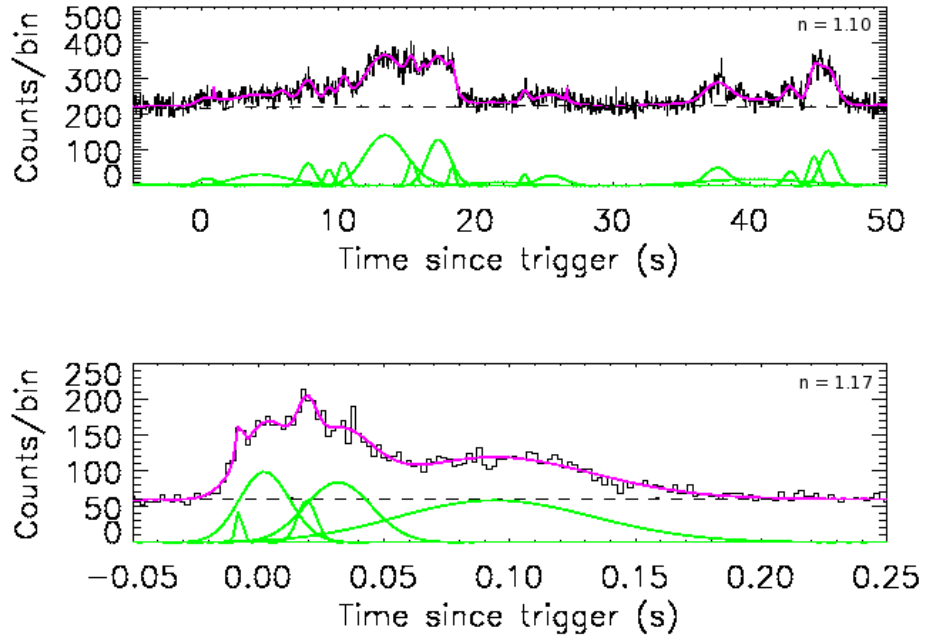


Fig. 2.— A sample pulse fit to one long burst GRB 080723D (upper plot) and one short burst GRB 090227B (lower plot). The histogram in black is the GRB light curve and the fitted background is shown as black dashed line. The pulses shown in green are the lognormal pulses fitted to those in the light curves. The sum of the background model and the fitted pulses is shown as purple continuous line. The goodness of fit parameter, n , is indicated at the top right corner of each plot.

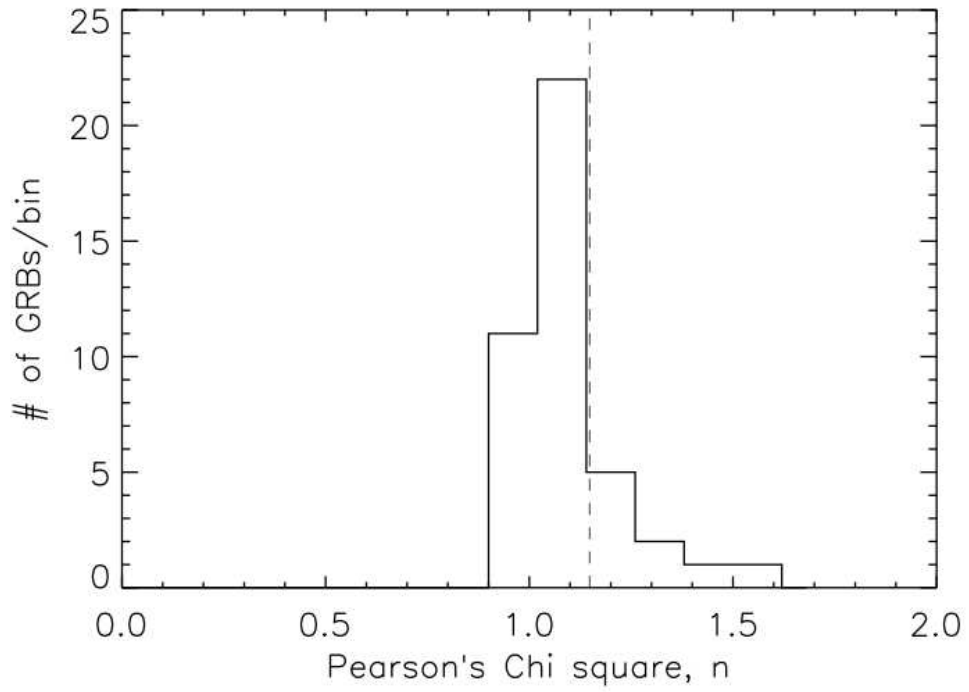


Fig. 3.— A distribution of the goodness of fit parameter n , viz. Pearson's chisquare estimated from the likelihood ratio for each fit. The vertical dashed line shows the mean value of the entire sample.

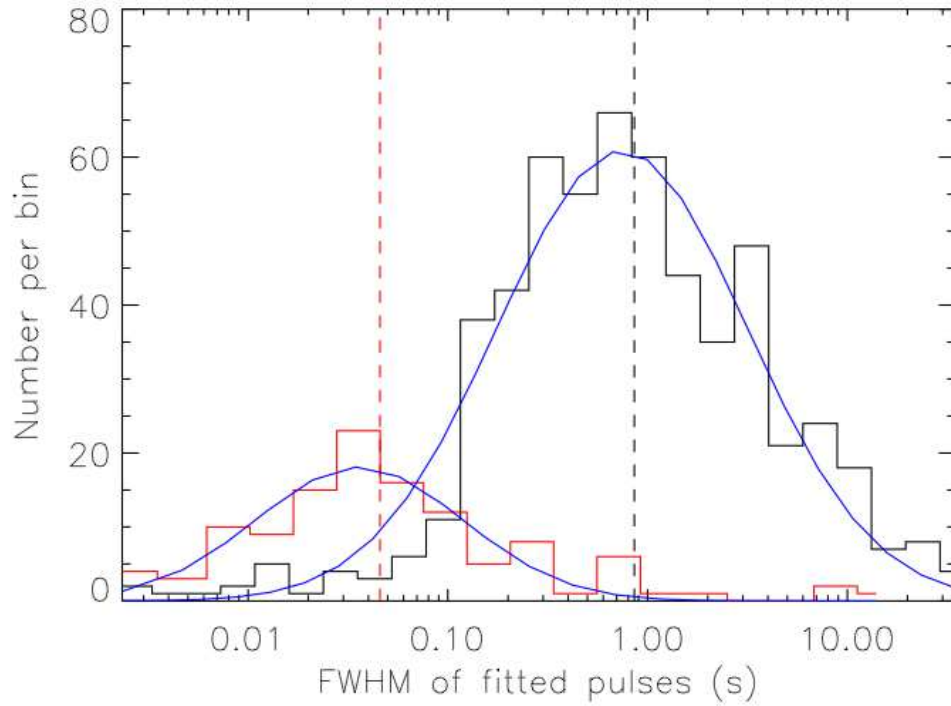


Fig. 4.— Distributions of the pulse widths (FWHM) for long (histogram shown in black) and short bursts (histogram shown in red). A lognormal function is fitted to each of the distributions. The mean values of FWHM (from the fit) for long and short bursts are 0.89 s and 0.055 s and the standard deviations are 5.2 s and 4.6 s respectively. The vertical dashed lines are the median values of FWHM for each class of GRBs.

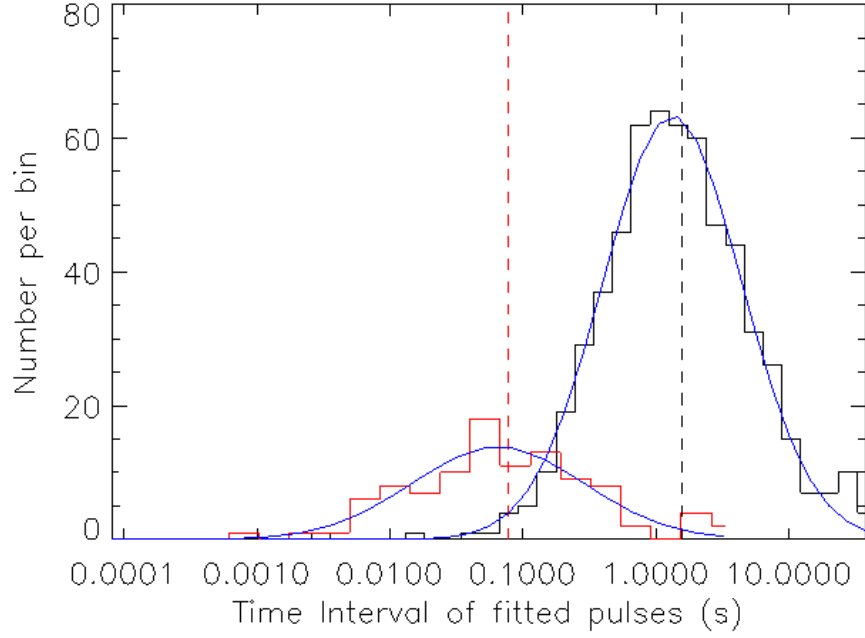


Fig. 5.— Distributions of the time intervals between successive pulses (Δt) for long (histogram shown in black) and short (histogram shown in red) bursts. A lognormal function is fitted to each of the distributions. The mean values of Δt (from the fit) for long and short bursts are 1.53 s and 0.076 s and the standard deviations are 3.6 and 5.1 respectively. The vertical dashed lines indicate the median values of the time intervals between successive pulses for each class of GRBs.

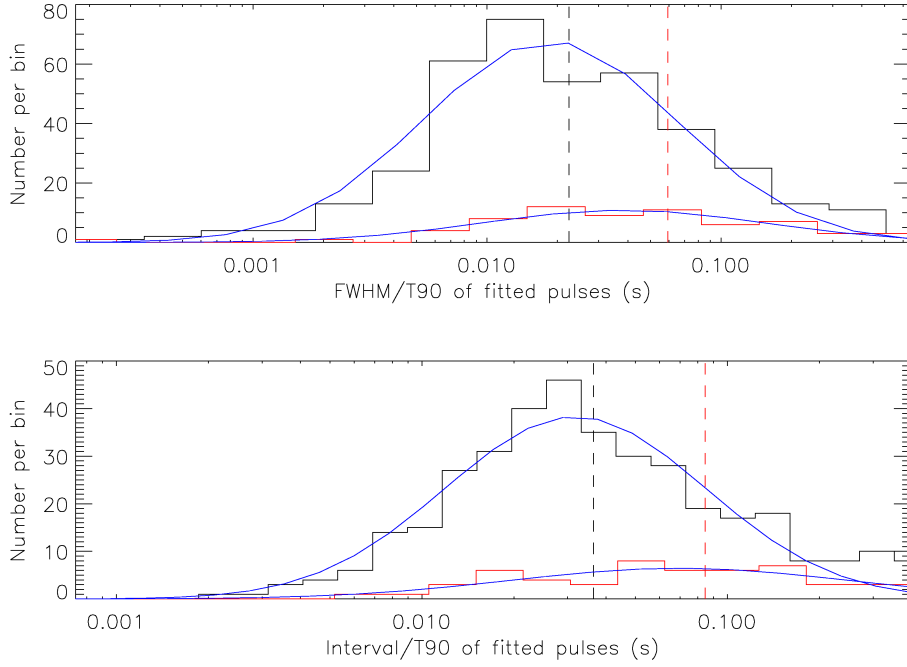


Fig. 6.— Distributions of the ratio of pulse widths (FWHM) of a burst to its total duration, T_{90} , for long bursts (histogram in black) and short bursts (histogram in red, upper panel). Each of the histograms is fitted with a lognormal function (shown as continuous curves in blue). The vertical dashed lines show the median values for long and short bursts respectively. The lower panel shows similar distributions of the ratio of the GRB time interval between successive pulses and the burst duration (T_{90}). Considering large errors in the short burst durations the two distributions may be considered to be consistent with each other in both the cases. The lag between the two distributions are 1.0 ± 0.7 (upper plot) and 2.0 ± 0.7 bins (lower plot)

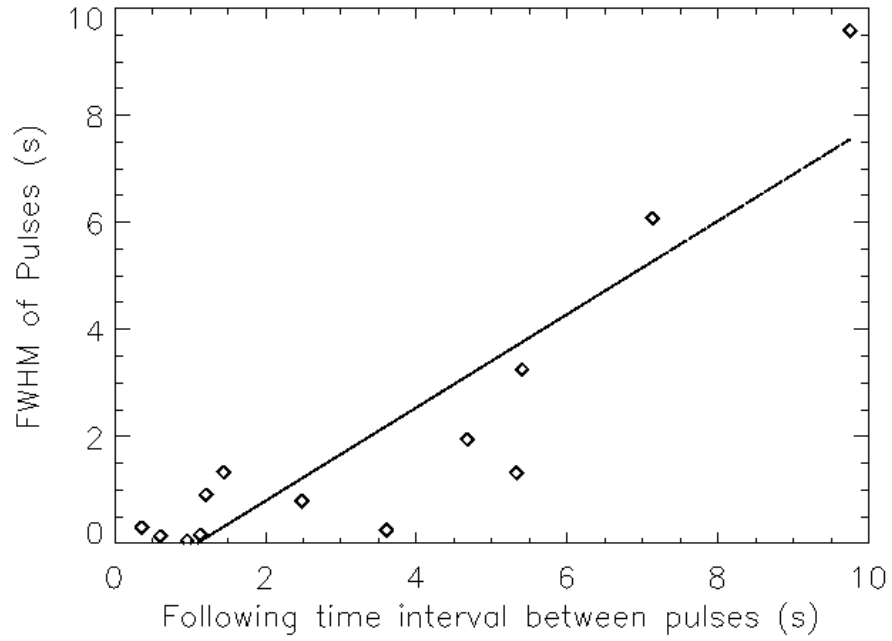


Fig. 7.— A plot of the pulse FWHM as a function of following time interval between successive separable pulses for a long burst GRB090626 which show a linear correlation coefficient of 0.896. The null hypothesis probability is 2.4×10^{-4} after taking into account of the number of GRBs searched (7 in this case). The black dashed line shows a linear fit to the data points.

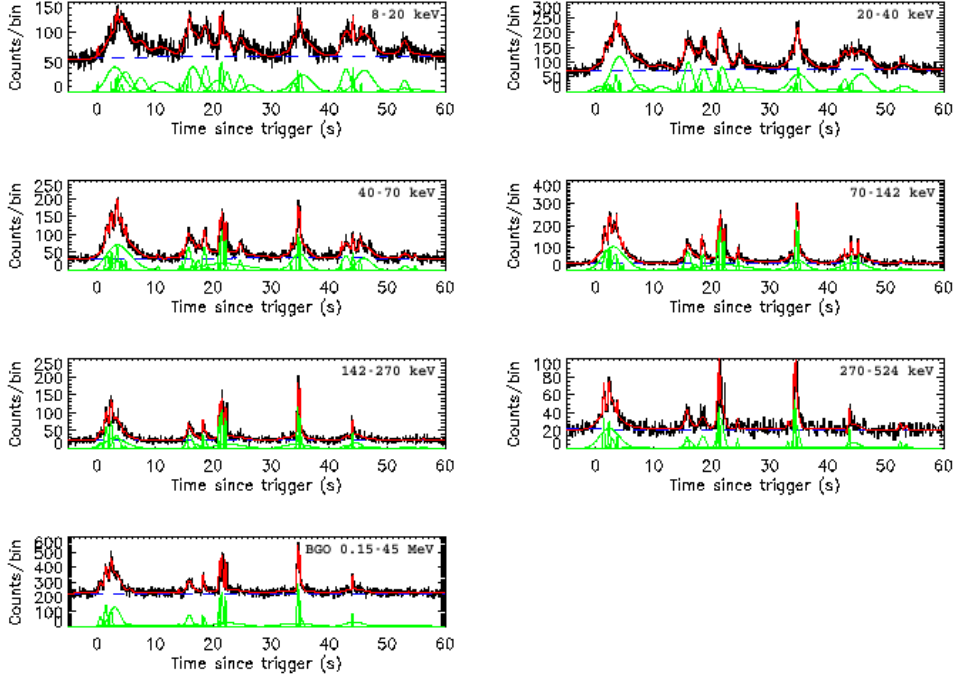


Fig. 8.— Sample pulse fits to the lowest 6 energy channels of NaI and the full energy range light curve from BGO detector of a long GRB 090626A. The histogram in black is the GRB light curve with a time resolution of 50 ms. The pulses shown in green are fitted lognormals to those in the GRB light curve. The horizontal dashed blue line is the fitted background while red curve is the fitted light curve resulting from summing the green and black curves. The temporal features in the light curve and hence the fitted pulses are narrower at higher energies.

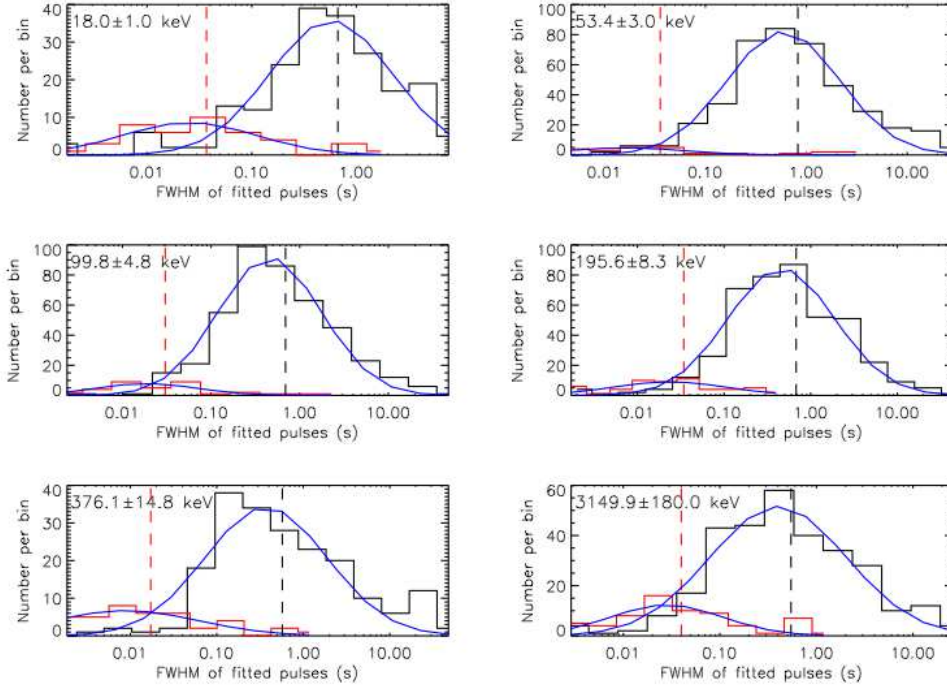


Fig. 9.— Evolution of the distributions of pulse widths for long (histogram shown in black) and short (histogram shown in red) GRBs as a function of energy. The first 5 distributions are from the NaI light curves in the first five energy bands as shown in Table 2. Also shown in the lowest right panel is a similar distribution for the total energy light curve from the BGO detector. The histograms for long and short bursts are fitted to lognormal functions and shown as continuous curves (in blue) in each energy band. The geometric mean energies corresponding to each plot are indicated in each panel. The errors on the mean energies are due to the finite energy resolution of GBM detectors.

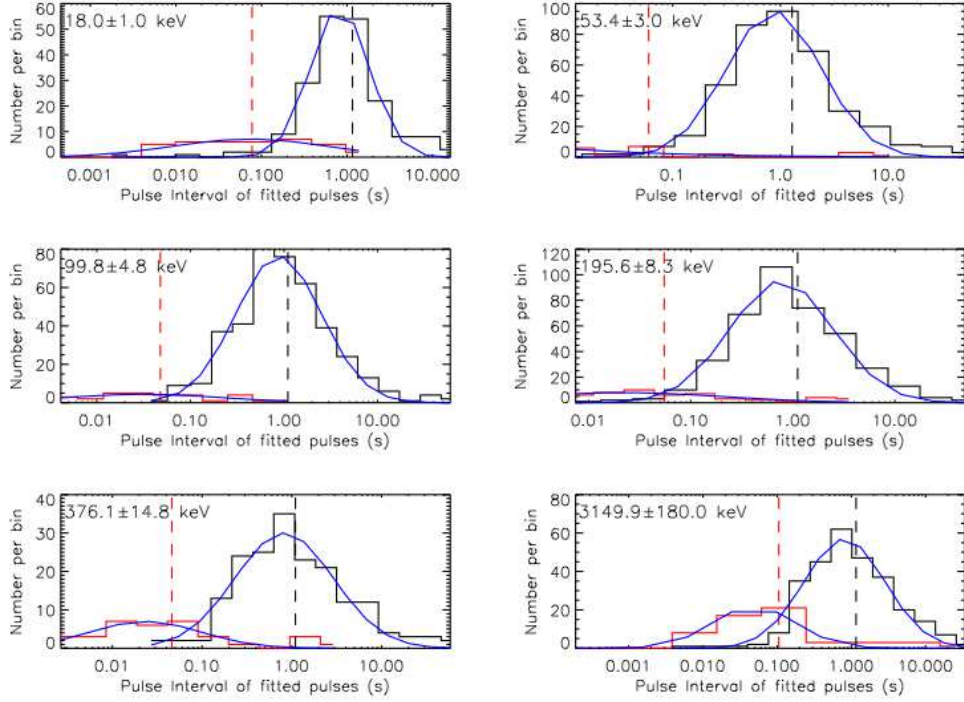


Fig. 10.— Evolution of the distributions of pulse time intervals between successive pulses for long (histogram shown in black) and short GRBs (histogram shown in red) as a function of energy. The first 5 distributions are from the light curves in the first five energy bands as shown in Table 2. Also shown in the lowest right panel is a similar distribution for the total energy light curve from the BGO detector. The histograms for long and short bursts are fitted to lognormal functions and shown as continuous curves (in blue) in each energy band. The geometric mean energies corresponding to each plot are indicated in each panel. The errors on the mean energies are due to the finite energy resolution of GBM detectors.

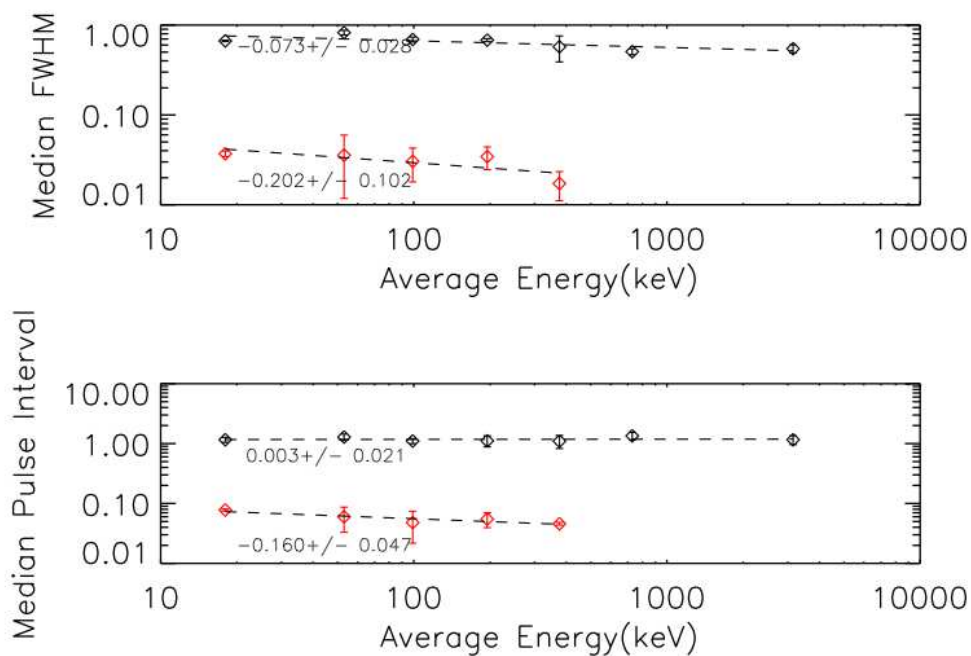


Fig. 11.— Evolution of the median pulse width (top) and median pulse intervals between successive pulses (bottom) for long and short GRBs with energy. The upper plot (in black) in each panel are the data for long bursts and the lower plot (in red) are for short bursts. In the case of short bursts both the pulse width and pulse interval show a faster decrease with increasing energy. In the case of long bursts on the other hand the pulse width shows a slower decrease with increasing energy than that for short bursts. The median pulse interval hardly seems to change with increasing energy in the case of long GRBs. The fitted power laws are shown as dotted lines for each type of GRBs and the fitted slopes are indicated.

REFERENCES

396

397 Aitchison, J. and Brown, J. A. C., 1969, “The Lognormal Distribution”, Cambridge
398 University Press.

399 Bissaldi, E. *et al.*, 2011, ApJ, 733, 97

400 Chiang, J., 1998, ApJ, 508, 752.

401 Daigne, F. and Mochkovitch, R., 2003, MNRAS, 587, 592.

402 Dermer, C. D. and Mitman, K. E., 1999, ApJ, 513, L5.

403 Dermer, C. D., 2004, ApJ, 614, 284.

404 Dermer, C. D. and Menon, G., “High Energy Radiation from Black Holes”, 2009, Princeton
405 University Press.

406 Eichler, D., Livio, M., Piran, T. and Schramm, D. N., 1989, Nature, 340, 126

407 Fenimore, E., in’t Zand, J. J. M., Norris, J. P., Bonnell, Nemiroff, R. J., 1995, ApJ, L101

408 Fenimore, E., Madras, C. D. and Sergei, N., 1996, ApJ, 473, 998

409 Fenimore, E., Ramirez-Ruiz, R. and Summer, M. C., 1997, Gamma-ray Bursts, 4th
410 Huntsville Symposium, Ed. Meegan, C., Preece, R. and Koshut, T., AIP Conf. Proc.,
411 NY, 428, 657.

412 Gehrels, N. *et al.*, 2005, Nature, 437, 851.

413 Göğüs, E., *et al.*, 2000, ApJ, 532, L121.

414 Guiriec, S., *et al.*, 2010, ApJ, 725, 225

- 415 Gupta, V., Dasgupta, P. and Bhat, P. N., 2000, Gamma-ray Bursts, 5th Huntsville
416 Symposium, Ed. Kippen, R., Mallozzi, R. M. and Fishman, G. J., AIP Conf. Proc.,
417 NY, 526, 215.
- 418 Hakkila, J. and Cumbee, R. S., 2008, Gamma-ray Bursts, 6th Huntsville Symposium, Ed.
419 Meegan, C. A., Gehrels, N. and Kouveliotou, C., AIP Conf. Proc., NY, 1133, 379.
- 420 Hakkila, J. and Preece, R. D., 2011, arXiv:1103.5434
- 421 Horváth, I., 2005, A&A, 392, 791.
- 422 Hurley K. J., McBreen B., Rabbette, M., Steel, S., 1994, A&A, 288, L49
- 423 Ioka, K and Nakamura, T., 2002, ApJ, 570, L21.
- 424 Katz, J. I., 1997, ApJ, 490, 663
- 425 Kobayashi, S., Piran, T. and Sari, R., 1997, ApJ, 490, 92
- 426 Kouveliotou, C., Meegan, C. A., Fishman, G. J., Bhat, N. P., Briggs, M. S., Koshut, T. M.,
427 Paciesas, W. S., and Pendleton, G. N., 1993, ApJ, 413, L101
- 428 Kocevski, D., Ryde, F. and Liang, E., 2003, ApJ, 596, 389.
- 429 Kumar, P., 2007, MNRAS, 376, L57.
- 430 Lee, A., Bloom, E. D. and Petrosian, V., 2000, ApJS, 131, 1.
- 431 Leo, W. R., “Techniques for Nuclear and Particle Physics Experiments” Springer-Verlag,
432 1994, pp190.
- 433 Li, H. and Fenimore, E., 1996, ApJ, 469, L115.
- 434 McBreen B., Hurley K. J., Long R., Metcalfe L., 1994, MNRAS, 271, 662.

- 435 McBreen S., Quilligan F., McBreen, B., Hanlon, L. and Watson, D., 2001, A&A, 380, L31.
- 436 Meegan, C. A., Lichti, G., Bhat, P. N., Bissaldi, E., Briggs, M. S., Connaughton, V., Diehl,
437 R., Fishman, G., Greiner, J., Hoover, A. S., van der Horst, A. J., von Kienlin, A.,
438 Kippen, R. M., Kouveliotou, C., McBreen, S., Paciesas, W. S., Preece, R., Steinle,
439 H., Wallace, M. S., Wilson, R. B., and Wilson-Hodge, C., 2009, ApJ, 702, 791
- 440 Mészáros, P., and Rees, M. J., 1993, ApJ, 405, 278.
- 441 Mészáros, P., 2006, Reports of Progress in Physics, 69, 2259.
- 442 Nakar, E. and Piran, T., 2002, ApJ, 572, L139.
- 443 Nakar, E. and Piran, T., 2002, MNRAS, 331, 40.
- 444 Nakar, E., 2007, Phys. reports, 442, 166.
- 445 Narayan, R., Paczynski, B. and Piran, T., 1992, ApJ, 395, L83
- 446 Norris, J. P., Nemiroff, R. J., Bonnell, R. J., Scargle, J. D., Kouveliotou, C., Meegan, C. A.,
447 Fishman, G. J., 1996, ApJ, 459, 393.
- 448 Norris, J. P., Bonnell, J. T., Scargle, J. D., Hakkila, J. and Giblin, T. W., 2005, ApJ, 627,
449 324.
- 450 Paciesas, W. S., *et al.*, 2011, “The Fermi GBM Gamma-Ray Burst Catalog: The First Two
451 Years” (in preparation)
- 452 Preece, R. D., *et al.*, 2000, ApJS, 126, 19
- 453 Quilligan F., McBreen, B., Hanlon, L., McBreen, S., Hurley, K. J. and Watson, D., 2002,
454 A&A, 385, 377.
- 455 Quilligan F., Hurley K. J., McBreen B., Hanlon L., Duggan P., 1999, A&AS, 138, 419.

- 456 Racusin, J. L., 2008, *Nature*, 455, 183.
- 457 Ramirez-Ruiz, R. and Fenimore, E., 2000, *ApJ*, 539, 712.
- 458 Rees, M. and Mészáros, P., 1994, *ApJ*, 430, L93.
- 459 Sari, R. and Piran, T., *ApJ*, 485, 270.
- 460 Woosley, S. E. and Heger, A., 2006, *ApJ*, 637, 914
- 461 Woosley, S. E. and Bloom, J. S. 2006, *ARA&A*, 44, 507
- 462 Zhao, X., Li., Z. and Bai, J., 2011, *ApJ*, 726, 89